***PREPRINT**: Energy and Buildings, In press. doi:10.1016/j.enbuild.2009.12.010*

Uncertainty in airflow rate calculations due to the use of surface-averaged pressure coefficients

D. Cóstola[1a], B. Blocken[a], M. Ohba[b], J.L.M. Hensen[a]

(a) Building Physics and Systems, Eindhoven University of Technology, the Netherlands
(b) Tokyo Polytechnic University, Japan

Abstract

Mean wind pressure coefficients (C_p) are key input parameters for air infiltration and ventilation studies. However, building energy simulation and stand-alone airflow network programs usually only provide and/or use a limited amount of C_p data, which are based on several assumptions. An important assumption consists of using surface-averaged C_p values instead of local C_p values with a high resolution in space. This paper provides information on the uncertainty in the calculated airflow rate due to the use of surface-averaged C_p data. The study is performed using published empirical data on pressure coefficients obtained from extensive wind tunnel experiments. The uncertainty is assessed based on the comparison of the airflow rate (ϕ) calculated using the surface-averaged C_p values (ϕ_{AV}) and the airflow rate calculated using local C_p values (ϕ_{LOC}). The results indicate that the uncertainty with a confidence interval of 95% is high: $0.23\ \phi_{AV} < \phi_{LOC} < 5.07\ \phi_{AV}$. In cases with the largest surface-averaged ΔC_p, the underestimation or overestimation is smaller but not negligible: $0.52\ \phi_{AV} < \phi_{LOC} < 1.42\ \phi_{AV}$. These results provide boundaries for future improvements in C_p data quality, and new developments can be evaluated by comparison with the uncertainty of the current methods.

Keywords: wind pressure coefficient, surface averaging, uncertainty, Building Energy Simulation (BES), Air Flow Network (AFN) program, sensitivity, error, ventilation, infiltration.

1. Introduction

Air infiltration and ventilation play an important role in the energy performance of buildings as well as in the health, comfort and performance of the users [1-3]. Air infiltration and ventilation can be driven by different forces or systems, such as mechanical systems, buoyancy and/or wind [4]. The last one, in particular, involves complex phenomena, therefore, the calculation procedures of wind-driven ventilation and infiltration are often simplified, and thus introduce uncertainty in the analysis [5,6]. These simplifications are introduced in several aspects of the calculation such as: the wind data [7], the calculation method [8,9], the characteristics of openings and cracks [10,11] and the wind pressure distribution over the building facades [5,6,12]. The uncertainty due to the last one is addressed in this study.

In air infiltration and ventilation studies, wind pressure is usually represented by mean (i.e. time-averaged) wind pressure coefficients (C_p), which are defined as follows:

$$C_p = \frac{P_x - P_0}{P_d} \quad ; \quad P_d = \frac{\rho \cdot U_{ref}^2}{2} \qquad (1)$$

where P_x is the static pressure at a given point on the building facade (Pa), P_0 is the static reference pressure (Pa), P_d is the dynamic pressure (Pa), ρ is the air density (kg/m^3) and U_{ref} is the reference wind speed, which is often taken at building height h in the upstream undisturbed flow (m/s).

C_p data can be obtained from several primary and secondary sources [12]. Primary sources, such as full-scale experiments, reduced-scale experiments in wind tunnels and computational fluid dynamics (CFD) simulations, can provide custom and detailed C_p data for a specific building shape. However, obtaining these data is time-consuming and expensive, and they are seldom used in air infiltration and ventilation calculations [12]. Secondary sources, such as databases [1,13] or analytical methods [14-16] are very straightforward to use, therefore they are present in most of the programs used to perform air infiltration and ventilation calculations, such as Building Energy Simulation (BES) and stand-alone Air Flow Network (AFN) programs [12]. The drawback of secondary sources is the limited amount of C_p data provided and the related assumptions. An important assumption adopted by many secondary sources is the validity of using surface-averaged C_p values ($C_{p\text{-}AV}$) instead of local C_p values ($C_{p\text{-}LOC}$) with high resolution in space.

[1] **Corresponding author:** D. Costola
Building Physics and Systems, Eindhoven University of Technology, P.O. box 513, 5600 MB Eindhoven, the Netherlands. Tel.: +31 (0)40 247 2302, Fax +31 (0)40 243 8595, e-mail: d.costola@tue.nl

Based on recently published papers, it is possible to conclude that airflow calculations with $C_{p\text{-}AV}$ are considered reliable by many designers and researchers. $C_{p\text{-}AV}$ is used in approximately 8 out of 10 BES-AFN programs [12], and it is adopted by the scientific community to study a broad range of topics, such as double-skin facade performance [17], comparison between AFN and CFD [18], and single-sided ventilation [19]. Previous studies addressing the use of $C_{p\text{-}AV}$ were based on case studies, focusing on a particular building shape and configuration of openings/cracks, so the conclusions can not be generalized [20,21]. These previous works concluded that the surface-averaging process does not significantly reduce the accuracy of the airflow rate calculation [20,21]. Opposite to this, in the documentation of the widely used AFN program COMIS, Feustel et al. [22] state that "From experience we know that wall-averaged values of C_p usually do not match the accuracy required for air-flow calculation models.". In fact, several research efforts were conducted in the last decades to provide $C_{p\text{-}LOC}$ for air infiltration and ventilation studies [15,16,23].

Determining the reliability of using $C_{p\text{-}AV}$ is of particularly importance considering that, when air infiltration and ventilation are taken into account, C_p has been identified as one of the major sources of uncertainty in BES-AFN simulations [5,6]. Therefore, it is required to investigate the implications of using $C_{p\text{-}AV}$ instead of $C_{p\text{-}LOC}$. The results are useful for researchers, practitioners and BES-AFN software developers when choosing C_p data.

This paper quantifies the uncertainty in the calculated airflow rate due to the use of $C_{p\text{-}AV}$, considering 15 building shapes and a large amount of opening configurations. The focus is on wind-driven ventilation and infiltration, while buoyancy is not taken into account. The paper is organized as follows. Section 2 defines the relative airflow rate error and demonstrates how this error is influenced by the position of the openings in the facade. Section 3 briefly describes the wind tunnel data used in this paper. Section 4 presents the method and assumptions used to calculate the uncertainty, which provide results that are independent of the wind speed and the opening size/characteristics, for cases with two identical openings/cracks. Section 5 presents and discusses the calculated uncertainty, first in a detailed analysis of results for a cubic building model (Section 5.1), followed by the complete set of results (Section 5.2). Section 6 addresses the limitations of this research. Section 7 summarizes the main conclusions.

2. Relative airflow rate error

In this paper, the relative airflow rate error r for a specific pair of openings (i) is defined as:

$$r_i = \frac{\phi_{LOC} - \phi_{AV}}{\phi_{AV}} = \frac{\phi_{LOC}}{\phi_{AV}} - 1 \tag{2}$$

where ϕ_{LOC} is the airflow rate calculated from $C_{p\text{-}LOC}$ and ϕ_{AV} is the airflow rate calculated from $C_{p\text{-}AV}$. Based on wind tunnel results [24], Fig. 1(a) shows the histogram of $C_{p\text{-}LOC}$ values for the 5 faces of a cubic building model, where the wind is perpendicular to one face ($\theta = 0°$). Each facade has 100 equidistantly spaced data points and $C_{p\text{-}LOC}$ is related to U_{ref}. $C_{p\text{-}LOC}$ varies in a wide range, from -1.5 to 0.8 (stagnation pressure), while the distribution is far from homogeneous, showings peaks and gaps. Fig. 1(b) presents the histogram for $C_{p\text{-}AV}$, obtained from the same pressure data after the C_p surface-averaging process for each face. In this case, the data is reduced to 4 discrete values distributed over a smaller range. This reduction in the spectrum of C_p values due to averaging may lead to errors in the flow rate calculation. The relative error is a function of – among others – the position of the pair of openings, as exemplified in Figs. 2(a) and 2(b).

Fig. 2(a) shows the cube with a pair of identical openings, called i = 1. Fig. 2(a) also provides the distribution of C_p over two surfaces of the cube ($C_{p\text{-}LOC}$), as well as the averaged values ($C_{p\text{-}AV}$). For this specific pair of openings, the values of $C_{p\text{-}LOC}$ and $C_{p\text{-}AV}$ are the same. So, there will be no difference between the airflow rate calculated using $C_{p\text{-}AV}$ (ϕ_{AV_1}) and the one calculated using $C_{p\text{-}LOC}$ (ϕ_{LOC_1}). In this case, the ratio between ϕ_{LOC_1} and ϕ_{AV_1} is equal to 1, and the relative error (r_1) is 0, as expressed by Eqs. (3) and (4).

$$\frac{\phi_{LOC\_1}}{\phi_{AV\_1}} = 1 \tag{3}$$

$$r_1 = \frac{\phi_{LOC\_1}}{\phi_{AV\_1}} - 1 = 0 \tag{4}$$

Fig. 2(b) shows the same cube with another pair of openings, called i = 2. In this case, $C_{p\text{-}LOC}$ is quite different from $C_{p\text{-}AV}$; the real "local" pressure difference is larger than the surface-averaged one, therefore ϕ_{LOC_2} will be higher than ϕ_{AV_2} (Eq. (5)). In this particular case, the ratio between ϕ_{LOC_2} and ϕ_{AV_2} is equal to 1.5, and the relative error (r_2) is 0.5 (Eqs. 5 and 6), which implies that ϕ_{AV} underestimates $\phi_{LOC.}$

$$\frac{\phi_{LOC\_2}}{\phi_{AV\_2}} = 1.5 \quad (5)$$

$$r_2 = \frac{\phi_{LOC\_2}}{\phi_{AV\_2}} - 1 = 0.5 \quad (6)$$

The r value depends not only on the position of the openings, but also on the pressure distribution over the facade. In order to obtain representative results of r, this paper adopts the use of an extensive pressure distribution database from wind tunnel experiments [24]. These data will be briefly described in Section 3.

In general, the airflow rate, and consequently the r value, also depends on the characteristics of the openings and on the wind speed. However, for the particular case of two identical openings and considering some assumptions, it is possible to perform an evaluation of r that is independent of these factors, as explained in Section 4.

3. Wind tunnel experimental data

The "Tokyo Polytechnic University (TPU) wind pressure database" provided the experimental wind tunnel data used in this research (http://wind.arch.t-kougei.ac.jp/system/eng/contents/code/tpu) [24]. The database contains the results of tests carried out using PMMA (polymethylmethacrylate) models in a Boundary Layer Wind Tunnel with a test section 2.2 m wide by 1.8 m high. The atmospheric boundary layer was simulated by turbulence-generating spires, roughness elements and a carpet on the upstream floor of the wind tunnel's test section. Different wind profiles were used to build the database. In most experiments, the mean velocity (with power-law exponent α = 0.20) and the turbulence intensity profiles were in accordance with the category III (suburban terrain) in Ref. [25]. The turbulence intensity at a height of 10 cm was about 0.25, and the test wind velocity at this height was about 7.4 m/s [24]. The minimum building Reynolds number is 25 340, which is above the 11 000 threshold for Reynolds number independent flow [26]. Table 1 presents an overview of the wind tunnel test cases used in this paper, which covers 15 different building shapes, several roof pitches and wind directions (5 to 19 different directions were tested depending on the case). Considering the variations in the building geometry, wind attack angle, roof pitch and wind profile power-law exponent, a total of 145 wind tunnel tests are presented in Table 1. All these data are used in the present study.

4. Calculation method for the relative airflow rate error

As demonstrated in Section 2, the impact of the surface-averaging process on r depends on the position of the openings. Hence, the calculation of the value of r must be performed for a representative number of opening pairs. In addition to that, it would be desirable to isolate the effects of the surface averaging on the calculated flow rate from the effects of wind speed and characteristics of the openings/cracks. In order to achieve this goal and considering the wind tunnel data available for each building shape and wind direction, the r values were calculated using the following assumptions: (1) there is only one interior zone in the building (no internal partitions); (2) there are only two openings or cracks in the building envelope; (3) the two openings or cracks are not situated in the same facade (single-sided ventilation and single-sided infiltration are not considered); (4) the two openings/cracks have the same area A and the same discharge coefficient C_z, (5) buoyancy is not taken into account. In this case, the flow rates (ϕ) can be calculated with Eq. (7):

$$\frac{\phi_{LOC\_i}}{\phi_{AV\_i}} = \frac{U_{ref} \cdot A \cdot C_z \cdot \left(\left|\Delta C_{p-LOC\_i}\right|\right)^{0.5}}{U_{ref} \cdot A \cdot C_z \cdot \left(\left|\Delta C_{p-AV\_i}\right|\right)^{0.5}} \quad (7)$$

It is important to note that the following additional assumptions are implicit to Eq. (7): fully-developed turbulent flow expressed by the flow exponent 0.5, the pressure distribution on the building envelope is not affected by the presence of openings (sealed-body assumption), and the dynamic pressure in the room is negligible [27]. From Eq. (7) it is clear that r does not depend on the reference wind speed (U_{ref}) and on the opening characteristics (A and C_z). Therefore, Eq. (8) is used to calculate r in this study.

$$r_i = \sqrt{\frac{\left|\Delta C_{p-LOC\_i}\right|}{\left|\Delta C_{p-AV\_i}\right|}} - 1 \quad (8)$$

In this equation, $\Delta C_{p\text{-}AV}$ must be different from 0. It is therefore not suitable to evaluate the error in pairs of openings where $\Delta C_{p\text{-}AV}$ is near or equal to zero. This can apply to openings placed in the same facade and to openings placed in two facades which have the same or approximately the same $C_{p\text{-}AV}$, e.g. symmetric facades with regard to the wind direction. In order to exclude such cases, a minimum $\Delta C_{p\text{-}AV}$ threshold of 0.015 is used to discard these pairs of openings from the study. The number of possible remaining pairs varies depending on the case and the wind direction. For Case 1 (Table 1), for example, r was calculated for a total of 100 000 pairs of openings for most of the wind directions. For some wind directions with symmetric facades, the amount of pairs is slightly reduced. For $\theta = 0°$, only 90 000 pairs were retained (two symmetrical surfaces), while 80 000 pairs were retained for $\theta = 45°$ (both windward facades are symmetric as well as the leeward ones). For some wind directions, e.g. 10° and 30°, the roof and one leeward facade have about the same $C_{p\text{-}AV}$, therefore the number of pairs is also reduced to 90 000. The calculated r values were processed statistically and the results are presented in the following section.

5. Uncertainty in the calculated flow rate

5.1 Results for the cubic model

In this section, the results for Case 1 (Table 1) are presented and analyzed in detail. In this case, C_p on each face of a cubic model was measured at 100 points of an array of 10 by 10 equidistantly spaced points. Data are available for 10 wind directions, from 0° to 45°, with intervals of 5°.

Considering $\theta = 5°$, it is possible to define a total of 100 000 pairs of openings because for all faces $\Delta C_{p\text{-}AV}$ is larger than the threshold 0.015. Fig. 3 presents the probability density graph (kernel density estimation [28]) based on the 100 000 values of r, for $\theta = 5°$. As expected, the most probable errors are around zero. In these cases, the use of surface-averaged values does not lead to major errors in the airflow rate calculation. Despite the expected peak around r = 0, both the upper and lower tails show a large probability of high r value, i.e. large overestimations or underestimations in the calculated airflow rate. Fig. 6 also shows the limits for the confidence interval (CI) of 95%. Considering the amount of opening pairs used to construct this graph, this CI discards 2 500 pairs, in each tail. The lower bound for CI = 95% is -0.75. This means that ϕ_{AV} will be overestimating the real airflow rate (ϕ_{LOC}) by a factor 4. The upper bound is +3.70, so ϕ_{AV} will be underestimating ϕ_{LOC} by a factor 4.7. Fig. 3 presents results for only one wind direction, $\theta = 5°$. In the following graphs, the results for other directions are presented.

Fig. 4 shows the upper bound values for all wind directions, considering CI = 95%, where r varies from 0.53 to 3.87, i.e. underestimation of ϕ_{LOC} by ϕ_{AV} can occur for all wind directions. The values in Fig. 4 show a large variation, indicating that some wind directions are associated with higher r. From Eq. (8), it is possible to conclude that high r values may be associated with low $\Delta C_{p\text{-}AV}$, high $\Delta C_{p\text{-}LOC}$ or a combination of both. It was found that especially the low $\Delta C_{p\text{-}AV}$ can explain the variation of r values with the wind direction. Considering a building with 5 faces, such as the cubic model used in this section, there are only 10 possible values for $\Delta C_{p\text{-}AV}$, which are derived from the possible combinations of two surfaces. Fig. 5 shows the smallest of the 10 possible values of $\Delta C_{p\text{-}AV}$ for each wind direction, and the same trend as in Fig. 4 can be observed. For the cubic model, the pairs of openings with the smallest $\Delta C_{p\text{-}AV}$ have always one opening placed in the roof, the other opening is placed in one of the leeward facades. The windward facade does not play a role in these values. Another fact that can explain the high r values associated with $C_{p\text{-}AV}$ for this flat roof surface is the flow separation at the windward roof edge. This flow separation is responsible for a high variation of $C_{p\text{-}LOC}$ at the roof surface near this roof edge, and such variation cannot be captured by $C_{p\text{-}AV}$. In order to understand the influence of the roof in the results, the calculation of r was repeated considering only the vertical surfaces (i.e. excluding the roof), for approximately 60 000 opening pairs for each direction. Fig. 6 shows the resulting upper bound values for CI = 95%. The graph confirms that the highest values are associated with the roof, but the occurrence of high r values still persists if only the vertical surfaces are taken into account.

Concerning the lower bound, the values for all wind directions lie in a narrower range, as shown in Fig. 7. The maximum r is -0.76 for $\theta = 0°$, and overestimation of ϕ_{LOC} by ϕ_{AV} can occur for all directions. For the lower bound values, the impact of the roof is less pronounced than for the upper bound. From Eq. (8), it can be seen that the lower bound values can be associated with low $\Delta C_{p\text{-}LOC}$, with high $\Delta C_{p\text{-}AV}$, or a combination of both. Further analysis revealed that low $\Delta C_{p\text{-}LOC}$ values play a major role in the definition of the lower bound value. As for the upper bound, the windward facade is also not important in the lower bound value definition.

Openings at the windward facade are not related to the highest r values, but they are especially relevant in practice because pairs with one opening at the windward facade often represent the highest values of $\Delta C_{p\text{-}LOC}$ (and $\Delta C_{p\text{-}AV}$) and consequently the highest airflow rates. Fig. 8 presents the upper and lower boundaries, for CI = 95 % and for 10 wind directions, when only the pairs with an opening in the windward facade and the other in the roof are taken into account. These are the pairs with the largest $\Delta C_{p\text{-}AV}$, considering the 10 possible values for $\Delta C_{p\text{-}AV}$ which are derived from the possible

combinations of two surfaces for this cubic model. In this case, r is much lower than the values presented in the previous figures, but it is still very significant. The upper boundary indicates that ϕ_{LOC} is about 10 % to 50 % higher than ϕ_{AV}, while the lower boundary indicates that ϕ_{LOC} is about 10 % to 40 % lower than ϕ_{AV}. In both cases, the largest errors occur when $\theta = 45°$. The reason is that the range of $C_{p\text{-}LOC}$ values on the windward facade increases, leading to larger differences between $C_{p\text{-}LOC}$ and $C_{p\text{-}AV}$.

5.2 Results for different building shapes

Results for the 15 cases (Table 1) are presented in this section. In Section 5.1, the upper and lower bounds were provided for two scenarios: in the first scenario, all the possible pairs of openings were included in the analysis, while in the second one only the pairs with the largest $\Delta C_{p\text{-}AV}$ were included. It corresponds to the situation with one opening in the roof and one in the windward facade. In this section, only the cases with the largest $\Delta C_{p\text{-}AV}$ are presented, because they are the ones with the largest flow rate, for which the errors tend to be more relevant. Here, the largest $\Delta C_{p\text{-}AV}$ does not necessarily correspond to the situation with one opening in the roof and one in the windward facade.

Fig. 9 shows the upper and lower bounds of r values for each case as a function of the wind attack angle, when only the pairs with the largest $\Delta C_{p\text{-}AV}$ are taken into account, considering a CI of 95 %. The amount of wind directions tested for each case is represented in each graph of Fig. 9 by the marks on the x axis, e.g. Cases 3 and 6 show data for the same interval of wind directions, from 0° to 90°, however Case 3 shows data obtained for every 5° while Case 6 shows data obtained for every 15°. As described in Section 3, data from a total of 145 wind tunnel tests were used in this paper, i.e. Fig. 9 shows 145 values for the upper and lower bound of r values.

Some results and trends can be observed when comparing the results for the different cases in Fig. 9:

(i) The r values for flat roof buildings (Cases 1 to 6) tend to be higher than those for buildings with gable roof (Cases 7 to 15, excluding 13 which has a roof with very low slope);

(ii) The r values for buildings with gable roof also tend to be less sensitive to the wind attack angle;

(iii) The maximum r values, i.e. the highest relative errors, are found in Case 3, for both the upper bound (0.6; for $\theta = 85°$) and the lower bound (-0.5; for $\theta = 90°$);

(iv) The minimum r value, i.e. the smallest relative error, for the lower bound (-0.09) is found in Case 1 (for $\theta = 0°$), and for the upper bound (0.06) it is found in Case 15 (for $\theta = 0°$).

The actual explanation for observations (i) and (ii) cannot be obtained solely by the analysis of these data, however there are indications that both trends might be explained by the different edges where the flow separation occurs on flat and gable roofs. As described in the previous section, the flow separation on flat roofs occurs at the edge between the roof and the windward surface. Part of the flat roof near the separation edge is in direct contact with the flow region where high pressure gradients are present. Consequently, $C_{p\text{-}LOC}$ on this part of the roof assumes high negative values, which cannot be captured by $C_{p\text{-}AV}$. Opposite to this, the flow separation for gable roofs usually occurs at the roof ridge, and the magnitude and range of $C_{p\text{-}LOC}$ values at the leeward part of the roof are reduced. The maximum C_p value at the windward facade is reduced for the gable roof building, probably due to the wind blocking effect [29,30], which leads to reductions in $\Delta C_{p\text{-}LOC}$ and in the relative error. Another aspect that could explain observations (i) and (ii) is that the pressure distribution over the gable roof is represented by two surface-averaged values, one for each part of the roof, instead of a single value used for the whole flat roof, which reduces the error in the surface-averaging process. Nevertheless, the analysis of Case 13 in Fig. 9 indicates that the flow separation seems to play a much more important role than the division of the roof in two parts. In Case 13, the roof pitch is very low, so it can be expected that the separation occurs as if it were a flat roof case. In fact, the magnitude of the r values in Case 13 is comparable to the cases with flat roof (Case 1 to 6), confirming that the roof type/flow separation is important and also indicating that the division of the roof in two parts does not reduce significantly the r values.

Observations (iii) and (iv) indicate that there is a large variation in the upper and lower bounds of r values, depending on the building shape and wind attack angle. Ideally, users of surface-averaged C_p should have the information about the uncertainty (e.g., r value) related to the data they are using, however in practice this is not the case and most of the data available do not provide any information about it. Based on the total sample (i.e. total amount of data from all 145 wind tunnel tests) described in Table 1, result (iii) could be used to state that the upper and lower bound for r values are in the worse case between -0.5 and 0.6. This would provide an interval to be used by practitioners in uncertainty analysis. Although useful, this interval is based only on the extreme values which might be rarely found in practice. A more conservative approach is to neglect the upper and lower extreme values, and cover only 95% of the 145 tests that constitute the sample (i.e. CI = 95%). In this case, a lower bound of -0.48 and an upper bound of 0.42 are found. Substituting these r values in Eq. (2), the following relation between ϕ_{LOC} and ϕ_{AV} can be constructed: $0.52\ \phi_{AV} < \phi_{LOC} < 1.42\ \phi_{AV}$. These values, which consider only the pairs of surfaces with the largest $\Delta C_{p\text{-}AV}$, constitute the main result of the present study. If all surfaces are taken into account, instead of using only the pairs of surfaces with the largest $\Delta C_{p\text{-}AV}$, the uncertainty is much larger: $0.23\ \phi_{AV} < \phi_{LOC} < 5.07\ \phi_{AV}$

6. Discussion

Air infiltration and ventilation influence the performance of the buildings in several aspects, e.g. energy consumption, indoor air quality, thermal comfort and user productivity. Although there are studies that have presented a coupled approach for the simulation of outdoor wind flow and indoor natural ventilation of buildings [31], by far most wind-driven airflow studies are performed in a decoupled way. In these studies, the indoor airflow is driven by pressure coefficients imposed at the openings. These pressure coefficients are a key input parameter and very often, surface-averaged values are used. Considering the importance of this topic, the goal of the present study was to stress the influence of surface-averaged wind pressure data on the airflow rate calculation and to provide a quantitative indication of the potential error/uncertainty related to the use of surface-averaged pressure coefficients.

In spite of the efforts to provide a comprehensive description of the uncertainty in the calculated airflow rate due to the use of surface-averaged C_p, this study has a number of limitations, which are briefly mentioned below.

- As any study of this type, the range of experimental data presents the most relevant constraint to the generalization of the conclusions. In this case, the number of building shapes can be considered high, but is certainly far from the variety of shapes found in real buildings, especially because all buildings adopted in this study were isolated/unsheltered. In sheltered building situations, the variation of C_p over the surface can be expected to be lower, so the surface averaging would lead to a lower error as well.
- The number of openings is limited to two due to the methodology adopted. The use of more openings will render the problem dependent on the wind speed, the area of the openings and the value of the discharge coefficients. In this case, results are more difficult to obtain and more difficult to present. For cases with several openings, it seems more appropriate to perform the uncertainty analysis for the building under study, using Monte Carlo simulation for example, rather than to try to obtain general values for the calculated airflow rate like these presented here. Multi-zone problems face the same situation.
- The method presented in this paper is also not suited for the uncertainty analysis of combined wind and buoyancy. As mentioned above, conventional methods for uncertainty assessment can be used to address more complex and realistic cases. The main advantage of the present method is that the results provided are independent of the wind speed and the characteristics of the openings.
- Concerning the distribution of openings on the facade, the grid spacing adopted was that defined by the wind tunnel data available. The grid resolution certainly has an effect on calculation for points near the edges, where extreme C_p values occur. However, they are not common positions for openings, so it is assumed that the grid resolution should not significantly affect the uncertainty results presented here.
- For openings with exponents other than 0.5, e.g. some crack models, the method can also easily be applied. From Eq. 7, it is clear that the higher the exponent, the higher will be the influence of C_p in the calculated airflow rate.
- Another aspect regarding the opening description is the assumption that both openings have the same discharge coefficient C_z. There have been several demonstrations that C_z depends on the external flow, i.e. even geometrically identical openings perform differently depending on their relative orientation to the wind direction [10,11]. BES and AFN programs do not consider this phenomenon, so the assumption adopted here is at the same level as that of the state of the art airflow calculation programs, although it might need to be reconsidered in the future.
- This paper has only addressed the uncertainty on C_p data due to surface averaging. Secondary C_p data sources might adopt additional simplifications which are discussed in Ref. [12] and briefly summarized in Table 2. Therefore, the overall uncertainty can be higher than the values presented here. Future studies should address the overall uncertainty of different C_p data sources, such as databases, empirical models and CFD. For models that adopt surface-averaging, the results of the present study should be used to assess the importance of this assumption in the overall uncertainty of the model results.

7. Conclusions

This paper has presented an estimation of the uncertainty in the calculated airflow rate due to the use of surface-averaged C_p, for buildings with two identical openings and one internal zone, based on a wide range of building shapes and wind attack angles. The paper has also introduced a straightforward method to quantify this uncertainty, which provides results independent of the opening/crack characteristics and wind speed. The main conclusions are:

1. The uncertainty in the calculated airflow rate using surface-averaged pressure coefficients for an isolated building with two openings is $0.23\ \phi_{AV} < \phi_{LOC} < 5.07\ \phi_{AV}$; for a confidence interval of 95%. This large relative uncertainty is associated with small $\Delta C_{p\text{-}AV}$ or $\Delta C_{p\text{-}LOC}$, i.e. small airflow rate.
2. When only the surfaces with the largest $\Delta C_{p\text{-}AV}$ are considered, i.e. the largest airflow rates calculated using the averaged data, the uncertainty is reduced to $0.52\ \phi_{AV} < \phi_{LOC} < 1.42\ \phi_{AV}$.

The magnitude of the uncertainty is high, but the judgment about the usability of this data depends on the problem under analysis and the chosen performance indicator.

The results provide boundaries for future improvements in the C_p data quality. New developments can be evaluated by comparison with the uncertainty of the current methods.

Acknowledgements

This research is funded by the “Institute for the Promotion of Innovation by Science and Technology in Flanders” (IWT-Vlaanderen) as part of the SBO-project IWT 050154 “Heat, Air and Moisture Performance Engineering: a whole building approach”. This financial contribution is highly appreciated.

The authors also acknowledge the GCOE Program of the Tokyo Polytechnic University, for making the wind tunnel data available and for funding the Internship program in which this work was partially developed.

References

[1] M.W. Liddament, Air infiltration calculation techniques - an applications guide, AIVC, Bracknell, 1986.
[2] M. Santamouris, P. Wouters, Building ventilation – the state of the art, Earthscan, London, 2006.
[3] F. Allard (ed.), Natural ventilation in buildings: a design handbook, James x James, London, 1998.
[4] D. Etheridge, M. Sandberg, Building Ventilation: Theory and Measurement, Wiley, 1996.
[5] S. de Wit, G. Augenbroe, Uncertainty analysis of building design evaluations, Proceeding of the 7th International Building Simulation Conference, Rio de Janeiro, 2001.
[6] S. de Wit, Uncertainty in predictions of thermal comfort in buildings, PhD Thesis, Delft University of Technology, 2001.
[7] J. Wieringa, Does representative wind information exist?, Journal of Wind Engineering and Industrial Aerodynamics, 65 (1996) 1-12.
[8] D.W. Etheridge, Unsteady flow effects due to fluctuating wind pressures in natural ventilation design - mean flow rates, Building and Environment 35 (2000) 111-133.
[9] L. Wang, Q. Chen, Theoretical and numerical studies of coupling multizone and CFD models for building air distribution simulations, Indoor Air 17-5 (2007) 348–361.
[10] D. Cóstola, D.W. Etheridge, Unsteady natural ventilation at model scale - Flow reversal and discharge coefficients of a short stack and an orifice, Building and Environment 43 (2008) 1491-1506.
[11] T. Kurabuchi, M. Ohba, T. Goto, Y. Akamine, T. Endo, M. Kamata, Local dynamic similarity concept as applied to evaluation of discharge coefficients of cross-ventilated buildings – Part 1 basic idea and underlying wind tunnel tests; Part 2 applicability of local dynamic similarity concept; Part 3 simplified method for estimating dynamic pressure tangential to openings of cross-ventilated buildings, International Journal of Ventilation 4 (2005) 285-300.
[12] D. Cóstola, B. Blocken, J. Hensen, Overview of pressure coefficient data in building energy simulation and airflow network programs, Building and Environment 44 (2009) 2027-2036.
[13] M.L. Orme, N. Leksmono, AIVC Guide 5, AIVC, 2002.
[14] M.V. Swami, S. Chandra, Correlations for pressure distribution on buildings and calculation of natural-ventilation airflow, ASHRAE Transactions 94 (1988) 243–266.
[15] M. Grosso, Wind pressure distribution around buildings: a parametrical mode, Energy and Buildings 18 (1992) 101-131.
[16] B. Knoll, J.C. Phaff, W.F. de Gids, Pressure simulation program, Proceeding of the Conference on Implementing the Results of Ventilation Research, AIVC, 1995.
[17] M. Haase, F. Marques da Silva, A. Amato, Simulation of ventilated facades in hot and humid climates, Energy and Buildings 41 (2009) 361–373.
[18] O.S. Asfour, M.B. Gadia, A comparison between CFD and network models for predicting wind-driven ventilation in buildings, Building and Environment 42 (2007) 4079-4085.
[19] T.S. Larsen, P. Heiselberg, Single-sided natural ventilation driven by wind pressure and temperature difference, Energy and Buildings 40 (2008) 1031–1040.
[20] M.V. Swami, S. Chandra, Procedures for calculating natural ventilation airflow rates in buildings - Final Report FSEC-CR-163-86, Florida Solar Energy Center, Cape Canaveral, 1987.
[21] B.G. Wiren, Effects of surrounding buildings on wind pressure distributions and ventilation losses for single family houses – M85:19, National Swedish Institute for Building Research, Gavle, 1985.
[22] H.E. Feustel, B.V. Smith, V. Dorer, A. Haas, A. Weber, COMIS 3.2 - User Guide, Empa, Dubendorf, 2005.
[23] A.S. Eldin, A parametric model for predicting wind-induced pressures on low-rise vertical surfaces in shielded environments, Solar Energy 81 (2007) 52-61.
[24] Y. Quan, Y. Tamura, M. Matsui, S. Cao, A. Yoshida, TPU aerodynamic database for low-rise buildings. 12th International Conference on Wind Engineering, 2-6 July, Cairns, 2007.
[25] Architectural Institute of Japan, Recommendations for Loads on Buildings (in Japanese), Architectural Institute of Japan, 2004.
[26] W.H. Snyder, Guideline for Fluid Modeling of Atmospheric Diffusion, US Environmental Protection Agency, Report EPA-600/8-81-009, 1981.
[27] P. Karava, T. Stathopoulos, A.K. Athienitis, Wind driven flow through openings – a review of discharge coefficients, International Journal of Ventilation 3-3 (2005) 255-266.
[28] A. W. Bowman, A. Azzalini, Applied Smoothing Techniques for Data Analysis, Oxford University Press, 1997.
[29] B. Blocken, T. Stathopoulos, J. Carmeliet, A numerical study on the existence of the Venturi-effect in passages between perpendicular buildings, Journal of Engineering Mechanics - ASCE 134-12 (2008) 1021-1028.

[30] B. Blocken, J. Carmeliet, The influence of the wind-blocking effect by a building on its wind-driven rain exposure, Journal of Wind Engineering and Industrial Aerodynamics 94-2 (2006) 101-127.
[31] T. van Hooff, B. Blocken, Coupled urban wind flow and indoor natural ventilation modelling on a high-resolution grid: A case study for the Amsterdam ArenA stadium, Environmental Modelling & Software 25-1 (2010) 51-65.

Table 1. Overview of the wind tunnel tests

case number	number of wind directions tested	range of wind directions tested	roof type	roof pitch (°)	wind profile exponent	model dimensions W:D:H (mm)	model scale	equivalent full-scale height (m)
1	10	0° to 45°	flat	0	0.25	200:200:200	1/250	50.0
2	19	0° to 90°				200:100:200		
3	19					300:100:200		
4	10	0° to 45°				200:200:50		12.5
5	19	0° to 90°				170:120:50		
6	7				0.20	160:240:120	1/50	6.0
7	7		gable	26.6		160:160:120		
8	5					160:240:120		
9	7			45				
10	7			30				
11	7			21.8				
12	7			18.4				
13	7			4.8				
14	7			45		160:240:64		3.2
15	7			18.4				

Table 2. Simplifications associated with generic C_p data sources.

Factor that affects C_p	**Common simplifications**
Point of interest at the building facade surface	Surface-averaged data
Wind profile	Assumed profile parameters at the building site
Sheltering elements (e.g. buildings, trees)	Obstructions with generic shape (e.g regular array of boxes)
Building geometry and facade detailing	Generic data used for any building shape, and no facade details considered
Wind direction	Low angular resolution

Figure Captions

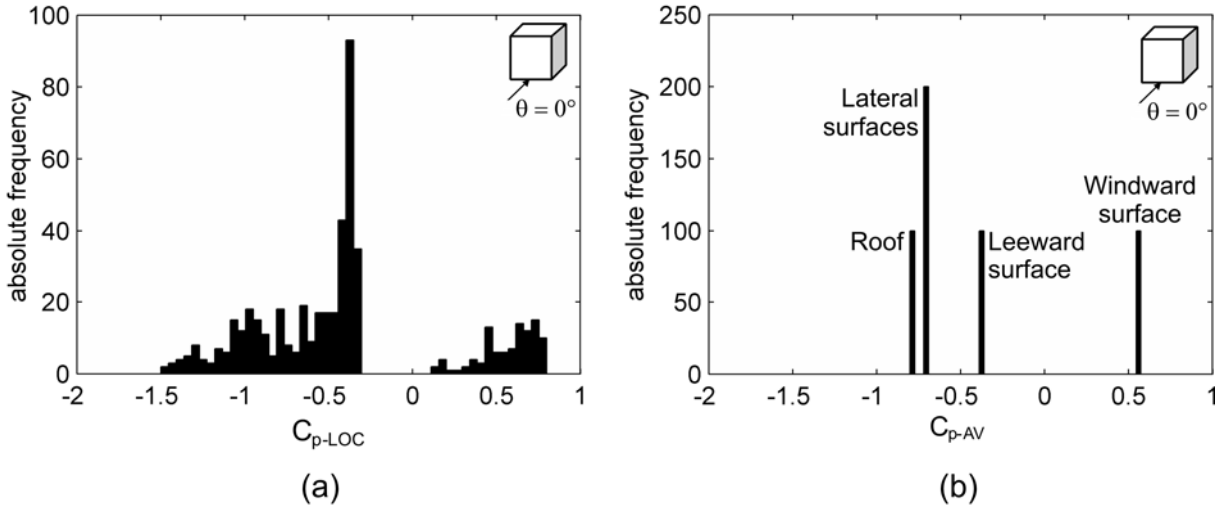

Fig. 1. (a) C_{p-LOC} histogram for a cube, θ = 0°, and (b) C_{p-AV} histogram for a cube, θ = 0°.

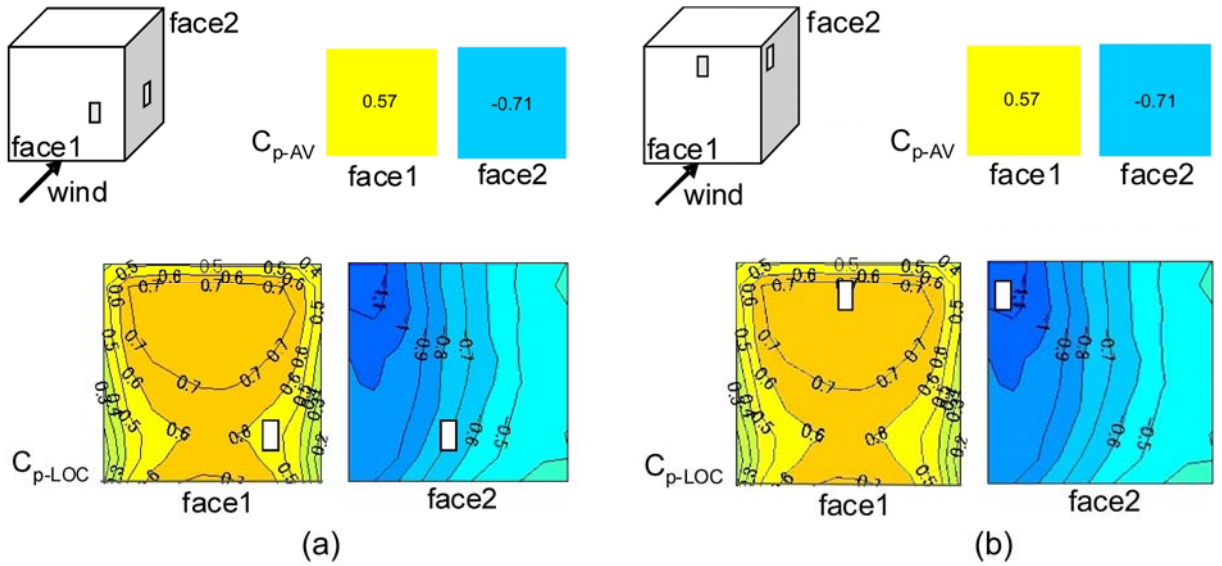

Fig. 2. (a) Case 1 - C_{p-LOC} and C_{p-AV} have the same value. (b) Case 2 - C_{p-LOC} and C_{p-AV} have different values (data from [24]).

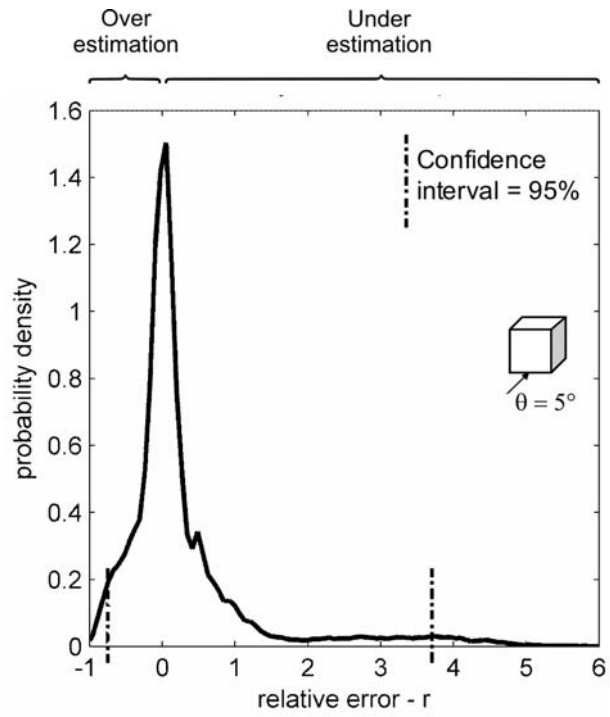

Fig. 3. Cubic model - probability density of r, θ = 5°.

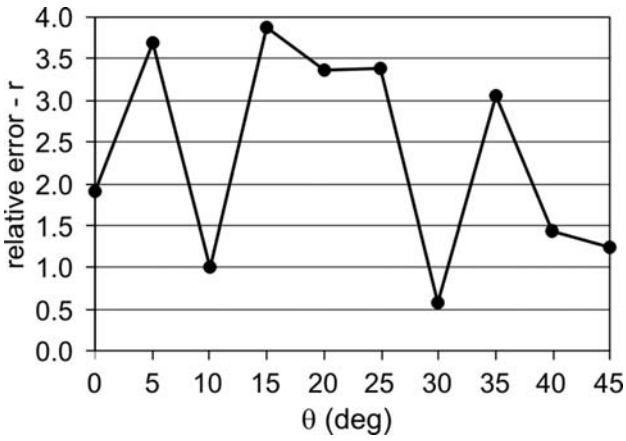

Fig. 4. Cubic model - Upper bound values of r ($\phi_{AV} < \phi_{LOC}$), CI = 95%.

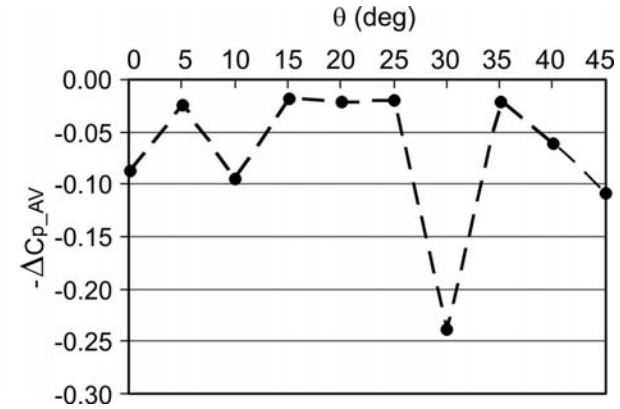

Fig. 5. Cubic model - Lower (absolute) ΔC_{p_AV} values.

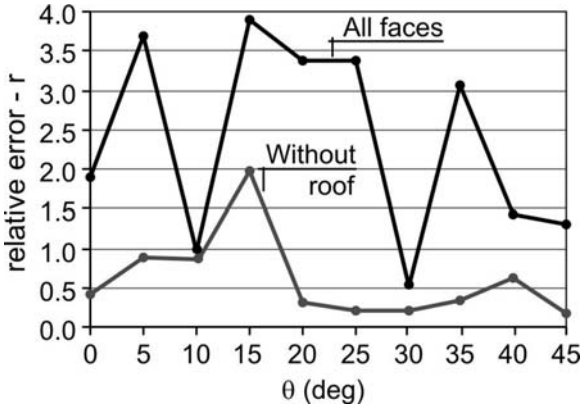

Fig. 6. Cubic model - Upper bound values of r ($\phi_{AV} < \phi_{LOC}$), CI = 95%.

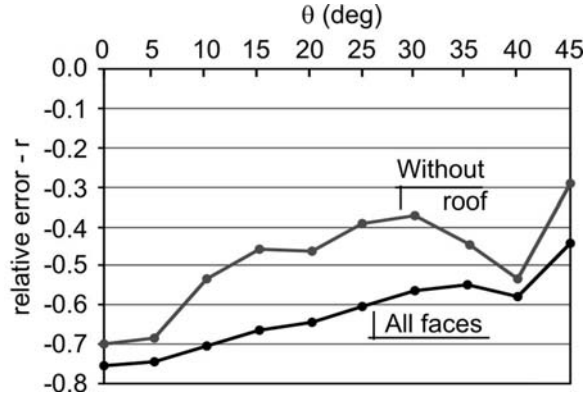

Fig. 7. Cubic model - Lower bound values of r ($\phi_{AV} > \phi_{LOC}$), CI = 95%.

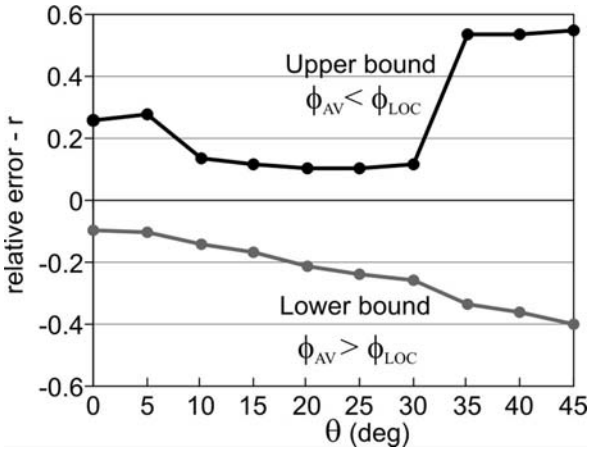

Fig. 8. Cubic model - Upper and lower bound values of r, when only pairs with the largest $\Delta C_{p\text{-}AV}$ are taken into account (one opening at the windward surface and the other at the roof; CI = 95%).

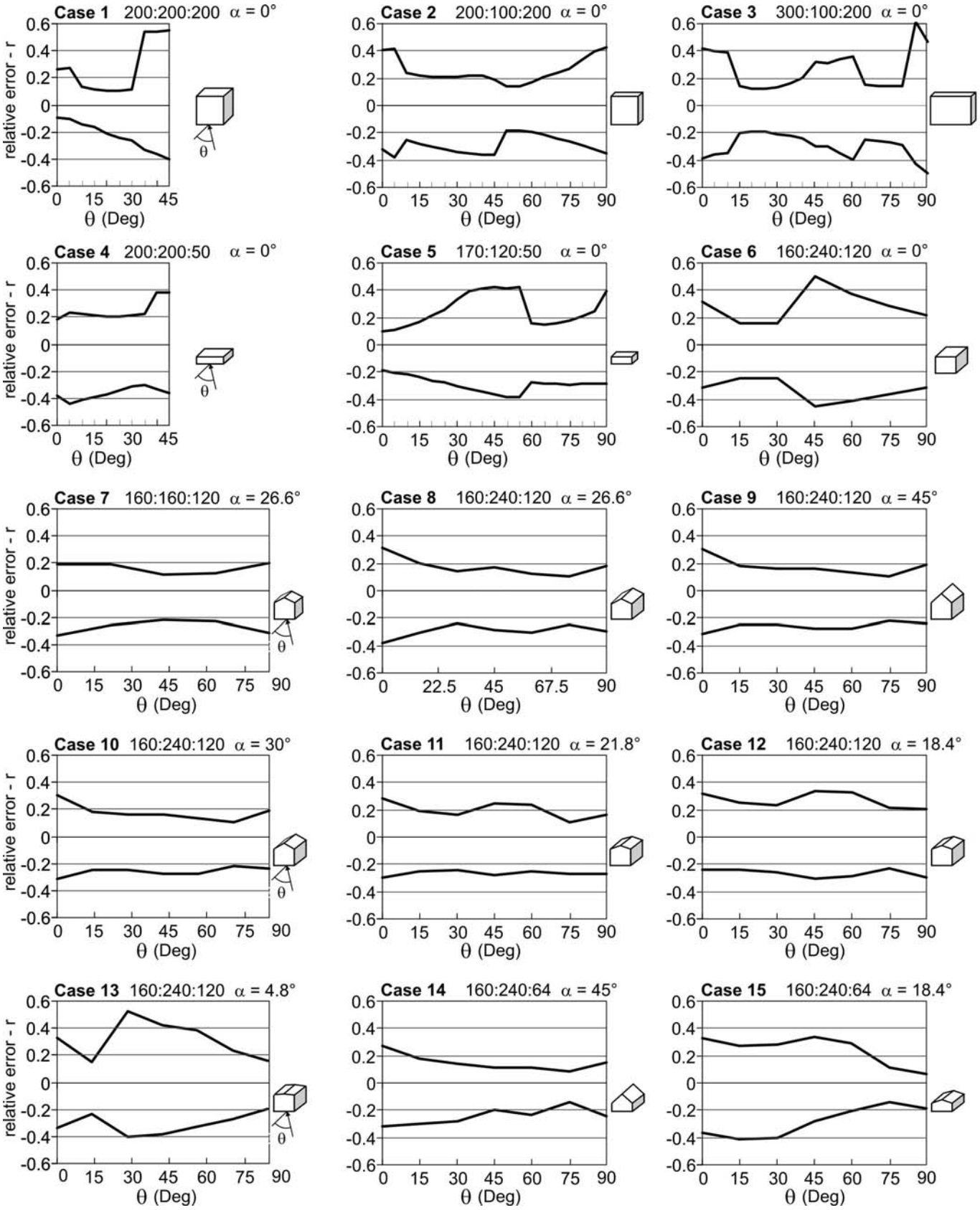

Fig. 9. Upper and lower bound values of r as a function of the wind attack angle, for CI = 95%, when only pairs with the largest $\Delta C_{p\text{-}AV}$ are taken into account, where α is the roof pitch.